Membrane and Water Treatment, *Vol. 11, No. 2 (2020)111-121*
DOI: https://doi.org/10.12989/mwt.2020.11.2.111

Performance of fouled NF membrane as used for textile dyeing wastewater

Mona A. Abdel-Fatah*, E.M.H. Khater, A.I. Hafez and A.F. Shaaban

National Research Center, Chemical Engineering and Pilot Plant Department, Cairo, Egypt

(Received October 14, 2018, Revised January 5, 2020, Accepted January 10, 2020)

Abstract. The fouling of Nanofiltration membrane (NF) was examined using wastewater containing reactive black dye RB5 of 1500 Pt/Co color concentrations with 16890 mg/l TDS collected from El-alamia Company for Dying and Weaving in Egypt. The NF-unit was operated at constant pressure of 10 bars, temperature of 25°C, and flowrate of 420 L/min. SEM, EDX, and FTIR were used for fouling characterization. Using the ROIFA-4 program, the total inorganic fouling load was 1.07 mM/kg present as 49.3% Carbonates, 10.1% Sulfates, 37.2% Silicates, 37.2% Phosphates, and 0.93% Iron oxides. The permeate flux, recovery, salt rejection and mass transfer coefficients of the dye molecules were reduced significantly after fouling. The results clearly demonstrate that the fouling had detrimental effect on membrane performance in dye removal, as indicated by a sharp decrease in permeate flux and dye recovery 68%. The dye mass transfer coefficient was dropped dramatically by 34%, and the salt permeability increased by 14%. In this study, all the properties of the membrane used and the fouling that caused its poor condition are identified. Another study was conducted to regeneration fouled membrane again by chemical methods in another article (Abdel-Fatah *et al.* 2017).

Keywords: membrane fouling; flux decline; nanofiltration; wastewater; ROIFA-4 software

1. Introduction

Nanofiltration (NF) is a process which removes organic compounds in the range of 300 to 1000 Dalton molecular weight cut-off, reject of the selected salts (i.e., divalent), and passing more water at lower pressure operations than RO systems. Membrane fouling phenomena present important limitations in the efficient application of NF technology. Fouling process results from the performance loss of a membrane due to: (i) deposition of substances whether they are suspended or dissolved substances on its opening pores of the external surfaces, (ii) the existence and growth of micro-living-organisms and (iii) irreversible collection of material (Organic + inorganic salts) on the membrane surface (Schaefer *et al*. 2005, Xu *et al*. 2006).

The membrane could be rapidly blocked by various kinds of fouling arising from the influent wastewater (Leo *et al*. 2016, Karisma *et al*. 2017, Chalor *et al*. 2007, Rabiller-Baudry *et al*. 2002, Abid *et al*. 2012, Thamaraiselvan and Noel 2015). A fouled membrane exhibits 2 key performance problems: higher than normal operating pressure and pressure drop. As the surface of the membrane becomes fouled with suspended solids that form another layer, which the feed water must penetrate to become permeate.

Membrane fouling decrease permeates flux as well as the recovery rate, increase operating costs, and shortens the membrane lifespan. Without proper wastewater pretreatment, rapid fouling may occur causing serious process deficiencies (Schneider *et al.* 2005).

Several factors may affect membrane fouling including: (i) membrane properties (material, pore size, hydrophobicity), (ii) solution properties (concentration, solute characteristics), (iii) operating conditions (pH, temperature, pressure, flow rate). The authors treated wastewater contaminated with reactive black dye-RB5 for 15 months by using NF membrane used in a previous article (Abdel-Fatah 2012). The partially fouled membrane is used in this article after proper cleaning to be used in an intensive fouling experiment. Throughout this article, the authors investigated the fouling phenomena of the NF membrane and its effect on the performance characteristics of NF separation using dyed wastewater.

2. Materials, tools, and methodology

2.1 Wastewater sources and characterization

Wastewater effluents contaminated with reactive black dye-RB5 from the cotton and the polyester dying fabrics in the dye-house effluent from El-alamia Company for Dying and Weaving in Egypt were used for fouling experiment by wastewater before and after fouling experiment the untreated and treated water were studied covering: pH, color, total suspended solids, total dissolved solids, chemical oxygen demand, cations (Ca^{2+}, Mg^{2+}, Ba^{2+}, Sr^{2+}, Na^{1+}, K^{1+}, Cu^{2+}, Mn^{2+}, Cr^{2+}, Al^{2+}, Zn^{2+} and Fe^{3+}); and anions (Cl^{1-}, F^{1-}, PO_4^{3-}, SO_4^{2-}, CO_3^{2-}, $HCO_3^{1-}$and SiO_3^{2-}). Analyses methods were carried out according to standard methods of analyses (Standard Methods 1992).

2.2 Experimental setup

Fig. 1 represents the experimental set up used. It is a

*Corresponding author, Ph.D.
E-mail: monamamin7@yahoo.com

Copyright © 2020 Techno-Press, Ltd.
http://www.techno-press.org/?journal=mwt&subpage=7
ISSN: 2005-8624 (Print), 2092-7037 (Online)

cross flow thin film NF bench scale unit, consisting of feeding tank, feeding pump, pre-filter cartridge (Model HYTRIX) of 5 micron polypropylene, automatic inlet shut-off valve, remote unit on/off capability, manometers (operating pressure gauge, low inlet pressure switch, conductivity meter), flow control center including concentrate and recycle valves, spiral wound NF module, stainless steel high-pressure pump, permeate and concentrate tanks and regulators. The NF membrane (Model E2 series with HL2521TF spiral wound module) of molecular weight cut off 150-300 Daltons (uncharged organic), active area 2.1 m^2. The module is of 53.3 cm length and 6.4 cm diameter. The maximum operating temperature is 50°C, the typical flux is 15-35 L/h.m^2. The NF design capacity is 1.68 m^3/d and the designed recovery is 33-50%. Typical operating pressure is 4.8 – 20 bars.

2.3 Experimental procedure

Dyed wastewater effluent with inlet TDS concentration of 16893 mg/L and color of 1500 Pt/Co is pumped into the NF set up. For fouling experiments, the following operating conditions were maintained over the fouling experiment until the membrane is completely blocked: pressure (10 bars), temperature (25°C), and flow rate (420 L/min). The permeate flux was monitored Membrane autopsy was used to identify the reasons for the loss in membrane performance. The clean and fouled membranes were cut into samples of size 5 mm × 5 mm. The fouled membrane is scratched and the resulted powder is examined.

2.4 Analytical and extmination Tests

The equipment and instruments used for investigated membranes (cleaned and fouled) were as follows: (1) Scan Electron Microscope (SEM) JEOL-JSM 6400 equipped with an Energy-dispersive X-ray spectroscopy (EDX) analysis system, (2) Fourier transform infrared spectroscopy (JASCO FTIR-6100, Japan), and (3) Hatch Spectro-photometer of DR-2800 model (for color intensity at a wavelength 400-800 nm) with frequencies between 4000 and 400 cm^{-1} and 4 cm^{-1} resolution).

3. Mass transfer in spiral wound modules

They are frequently two independent mathematical models: Eqs. (1)→(23) describe the fluid mechanics of water-permeate transport, salt flux, recovery and rejection factors, and how the mass transfer coefficient is calculated. Necessary equations are subsequently derived. On the other hand, Eq. (24) proves that: as the membrane porosity (ε) is decreased the effective diffusion coefficient (D^*) is also decreased. Eq. (25) proves the continuous decrease of the hindered mass transfer coefficient (k^*) with increasing the deposited cake thickness (δ_c).

As δ_c increases both the conventional and effective diffusion coefficients (D, D^*) are increased. This will result in increasing the fraction $(1/k^*,$ consequently: the hindered mass transfer coefficient (k^*) will be decreased. As fouling is increased (Eqs. (26) and (27)): The value of the term (α_i) is increased with decreasing permeate pressure. Permeate flux is affected by the product of (D_i) and $(K_i\alpha_i)$. The value added to $(K_i\alpha_i)$ be less than the value subtracted from (D_i). Eq. (28) presents the Sherwood number relating the mass transfer & division coefficient. Graphical presentation of the calculated $(K_w$ & $K_s)$ – finally Eqs. (29) and (30) reveal their continuous decline and increase with time respectively.

The solution diffusion models equations are successfully described steady state permeation of water flux (J_w) and solute flux (J_s) through diffusion controlled NF-membranes. SDM is utilized to predict permeate concentration (C_p), water and salt fluxes (J_w, J_s), % permeate recovery (%PR), solute mass transfer coefficient (k_s), and water and salt permeability (K_w, K_s). Mass balance equations for solvent and solute in the membrane module are written as (Rowe *et al*. 2010, Jyoti *et al*. 2015, Jiang *et al*. 2014, Lee *et al*. 2010, Jain *et al*. 2006, Zhao *et al*. 2005, Al-Aseeri *et al*. 2007)

$$Q_f = Q_c + Q_p \tag{1}$$

$$Q_f C_f = Q_c C_c + Q_p C_p \tag{2}$$

The water-permeate transport equations are given as

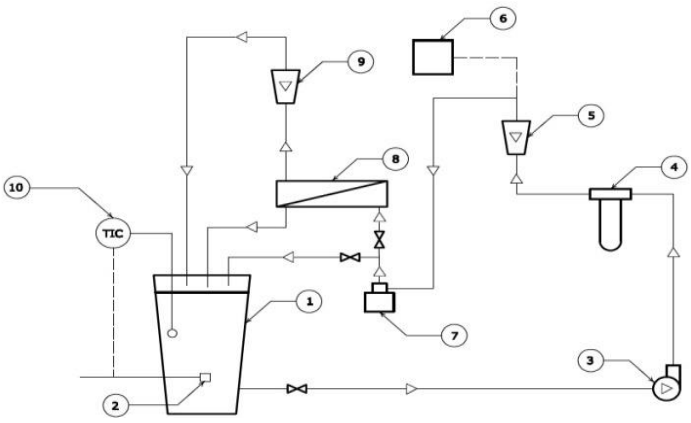

Fig. 1 Schematic flow diagram of NF-membrane separation system consists of (1) Feeding tank. (2) Electric heater. (3) Feeding pump. (4) Pre-filter. (5) Feed rotameter. (6) Conductivity meter. (7) High-pressure pump. (8) NF-membrane. (9) Permeate rotameter. (10) Temperature-indicator-controller

$$Q_p = (\Delta P - \Delta\pi)K_w A \quad (3)$$

Consequently, the permeate flux (J_p) is given by

$$J_p = \frac{Q_p}{A} = (\Delta P - \Delta\pi)K_w \quad (4)$$

The net hydraulic and osmotic pressure differentials across the membrane $(\Delta P, \Delta\pi)$ are mathematically expressed as (Rashidi *et al*. 2014, Xuan Nguyen and Van der Bruggen 2015, Chollom *et al*. 2015)

$$\Delta P = \bar{P} - P_p \quad (5)$$

$$\Delta\pi = \bar{\pi} - \pi_p \quad (6)$$

The average hydraulic and osmotic pressures on the feed side $(\bar{P}, \bar{\pi})$ are given as

$$\bar{P} = \frac{P_f + P_c}{2} \quad (7)$$

$$\bar{\pi} = (\pi_f + \pi_c)/2 \quad (8)$$

The rate of salt flow through the membrane is given by

$$M_s = (\bar{C} - C_p)K_s A \quad (9)$$

Consequently, the salt flux (J_s) is given by

$$J_s = \frac{M_s}{A} = (\bar{C} - C_p)K_s \quad (10)$$

The average salinity on the feed side $(\bar{C})$ is defined as

$$\bar{C} = \frac{(Q_f C_f + Q_c C_c)}{(Q_f + Q_c)} \quad (11)$$

The performance of a NF −membrane is determined by: solvent permeability (K_w), the recovery factor (%R), and rejection factor %(SR). The latter two parameters are expressed as

$$\% R = 100\left(\frac{Q_p}{Q_f}\right) \quad (12)$$

$$\% (SR) = 100\left(\frac{C_f - C_p}{C_f}\right) \quad (13)$$

The spacer composition used in the permeate and feed channels has shown a remarkable effect on the hydrodynamics inside spiral wound element. The spacer composition increases the effective velocity and decreases the void volume. The characteristic velocity in a spiral wound element is determined from the following equation (Amokrane *et al*. 2015, Murthy and Chaudhari 2009)

$$u_{eff} = \frac{U}{A_{eff}} \quad (14)$$

The effective area (A_{eff}) is a function of spacer thickness (h_{sp}), leaf width (b), and porosity (ε). The effective area (A_{eff}) is calculated from the following equation assuming that the effective channel height (h) is equal to the spacer thickness (h_{sp})

$$A_{eff} = bh\varepsilon \quad (15)$$

The hydraulic diameter (d_h) is calculated as follows for channels with periodically variable cross sections, such as spacer-filled feed and permeate channels

$$d_h = \frac{4\ x\ volume\ of\ flow\ channel}{netted\ surface} \quad (16)$$

While if a flat channel with spacer is used $(b >> h)$, the hydraulic diameter (d_h) is calculated as

$$d_h = \frac{4\,(V_{Tot} - V_{sp})}{(S_{Fc} + S_{sp})} \quad (17)$$

The porosity (ε) is calculated as

$$\varepsilon = \left(1 - \frac{V_{sp}}{V_{Tot}}\right) \quad (18)$$

And specific surface of the spacer $(S_{v,sp})$, and for flat channel

$$S_{v,sp} = \left(\frac{S_{sp}}{V_{sp}}\right) \quad (19)$$

The definition of the hydraulic diameter (d_h) becomes

$$d_h = \left\{\frac{4\varepsilon}{\left(\frac{2}{h}\right) + (1-\varepsilon)S_{v,sp}}\right\} \quad (20)$$

The effective cross flow velocity (u_{eff}) defined by Eq. (14) is now used to calculate the channel cross flow Reynolds number (Re_{eff}) expressed as

$$Re_{eff} = \frac{\rho u_{eff} d_h}{\mu} \quad (21)$$

The Schmidt number $(\boldsymbol{Sc})$ is defined as

$$Sc = \left(\frac{\mu}{\rho D}\right) \quad (22)$$

The mass transfer coefficient under laminar flow conditions is given by the following Eqs. (10)-(11) as (Abbas 2007, Mohammad *et al*. 2015, Masmoudi *et al*. 2014)

$$Sh = \left(\frac{kd_h}{D}\right) = 1.86\left\{Re_{eff}.Sc.\left(\frac{d_h}{L}\right)\right\}^{\frac{1}{3}} \quad (23)$$

4. Results and discussion

Membrane fouling is namely caused by precipitation and deposition of molecules or particulates on the membrane surface or membrane pores. The consequences of membrane fouling are increased membrane separation resistances, reduced productivity, severe flux decline, and/or

Table 1 Chemical analyses of wastewater before and after fouled NF membrane

Parameter	Feed water	Permeate water	Removal %	Conc. water	UNITS
Color	1500	29	98.1	2063	Pt/Co unit
pH	7.55	7.28		7.47	
COD	378	153	59.5	409	mg/l
BOD	215	90	58.1	210	mg/l
TSS	1123	46	95.9	1499	mg/l
TDS	16893	1534	90	22890	mg/l
Calcium (Ca^{++})	60	2.2	96.3	24.5	mg/l
Magnesium (Mg^{++})	48	15.9	66.9	23.4	mg/l
Sodium [Na^{+}]	3800	520	86.3	8550	mg/l
Potassium [K^{+}]	22	5	77.3	18	mg/l
Iron [Fe^{++}]	0.32	0.17	46.9	0.22	mg/l
Manganese [Mn^{++}]	0.08	0.02	75.0	0.06	mg/l
Strontium [Sr]	0.45	0.03	93.3	0.66	mg/l
Barium [Ba]	0.17	0.07	58.8	0.20	mg/l
Bicarbonate (HCO_3^{-})	2100	375	81.2	188	mg/l
Carbonate alkalinity as ($Ca\ CO_3$)	8.5	0.0	00.0	0.0	mg/l
Chloride [Cl^{-}]	1443	310	78.5	2997	mg/l
Sulphate [SO_4^{--}]	3200	200	93.8	4050	mg/l
Phosphate [PO_4]	5.4	0.98	81.9	19.4	mg/l
Silica [SiO_3]	15.8	1.44	72.2	36	mg/l

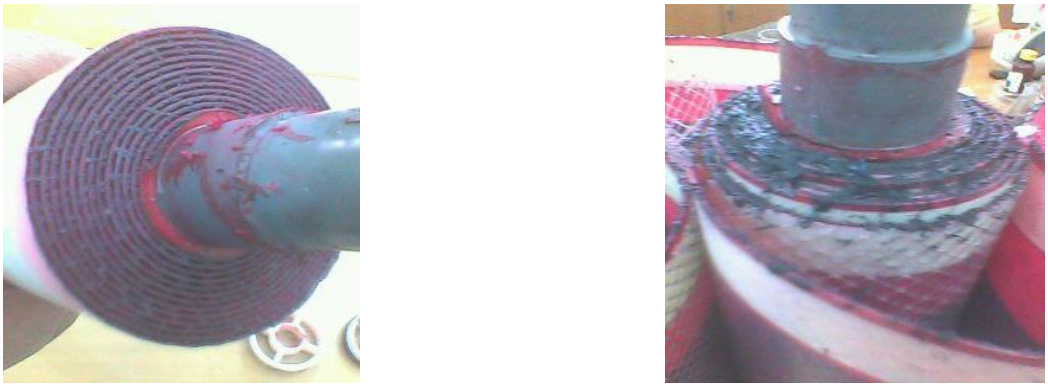

Fig. 2 Visual observation of the membrane module after NF- processing

altered membrane selectivity. Membrane fouling characterization is based on the type and nature of material being removed as: colloidal, organic, scaling, and bio-fouling. Each type of fouling and foulant has its effect on membrane performance and also has its own distinct mitigation/cleanup approach.

4.1 Water characterization

Chemical analyses of wastewater before and after fouled Nanofiltration membrane are presented in Table 1. It was observed that the removal% of TDS, TSS, COD, BOD, cations, and anion is decreased minimally after 10 hours, which means that the NF membrane is not working efficiently as a result of fouling.

4.2 SEM-EDS and IR results

The membrane module was visually inspected after 10 hours NF-processing, where fine hair cracks in the outer fiberglass skin were observed together with debris accumulation as shown in Fig. 2.

The dried cleaned and fouled membranes were analyzed with SEM (Scan Electron Microscope JEOL-JSM 6400) equipped with an EDX analysis system. Figs. 3(a)-(c) and (d); shows the profile of the NF membrane before after nanofiltration process for 720 minutes at magnified 200x, 500x, 1000x and 2000x by using SEM, where scanning with a focused beam of electrons was carried out at different scales. The distinctive difference between the virgin- and an exhausted membrane is approved by changes

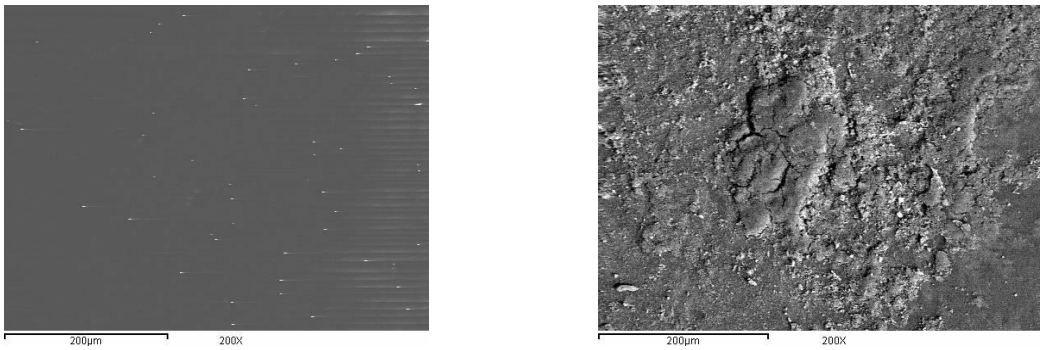

(a) SEM image of the membrane before and after fouling (scale 200x)

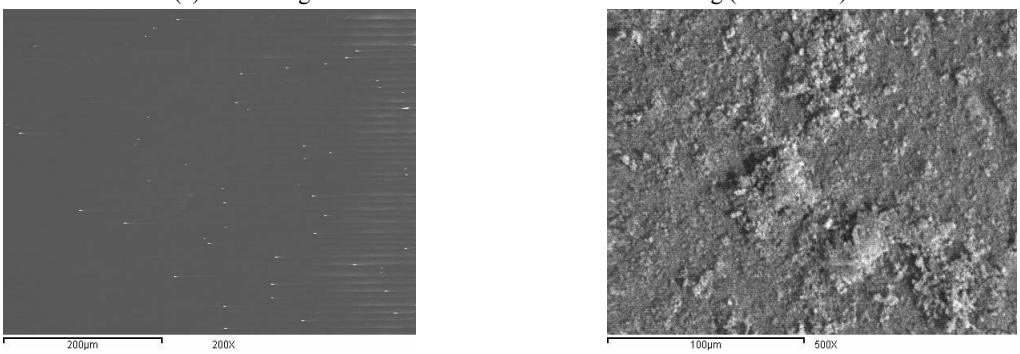

(b) SEM image of the membrane before and after fouling (scale 500x)

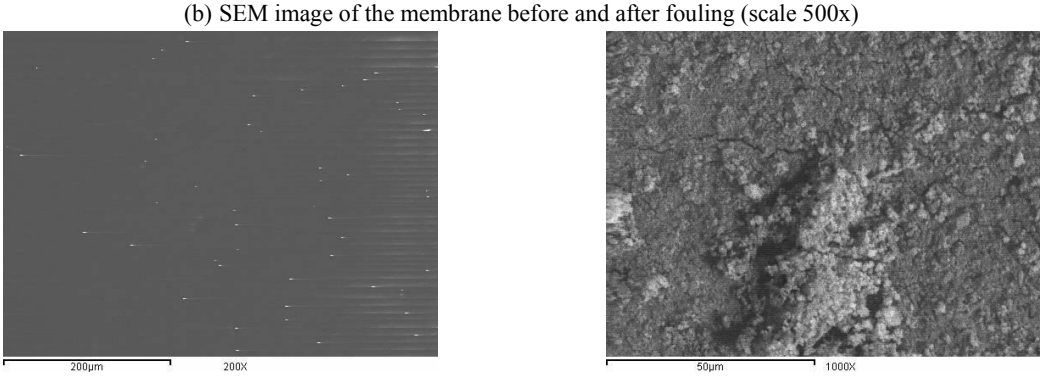

(c) SEM image of the membrane before and after fouling (scale1000x)

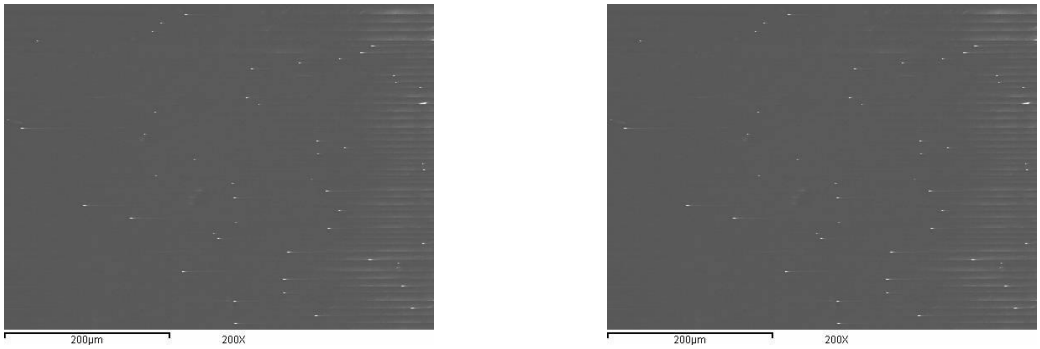

(d) SEM image of the membrane before and after fouling (scale2000x)

Fig. 3 SEM profile of the NF membrane

in surface topography and composition (morphology of deposits). Pore size of the NF membrane does not allow permeation of organic and silica colloids.

This is confirmed by the low turbidity of permeate samples. Spongy and coarse layer of $CaSO_4$ is crystallized and precipitated on the surface of membrane highlighting the foulant-foulant interactions. Dense and uniform cake layer colloidal silica is formed on the surface of membrane due to hydrophobic interactions between the foulant and membrane surface texture.

EDX is used as an analytical technique for the percentage of elemental composition analysis of the membrane. It is observed that the weight proportions of each element were 66.54% C, 27.43% O, and 6.03% S, which indicates the precipitation of solid $CaCO_3$ and $CaSO_4$ on the membrane surface as given in Table 2 and presented

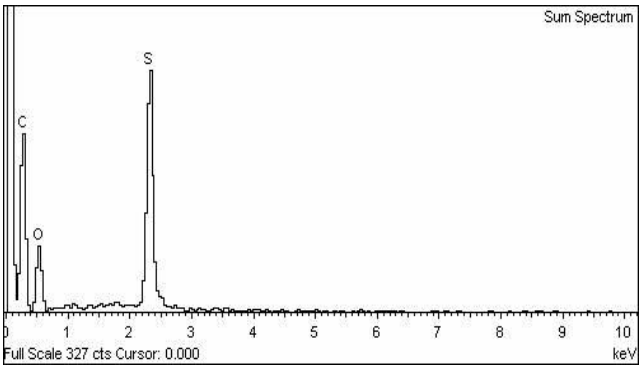

Fig. 4 Membrane EDX emission spectrum before fouling

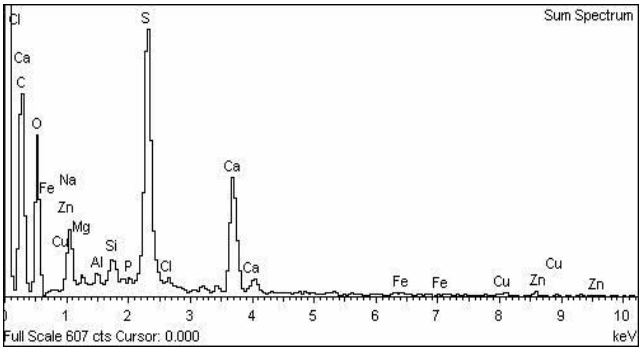

Fig. 5 Membrane EDX emission spectrum after fouling

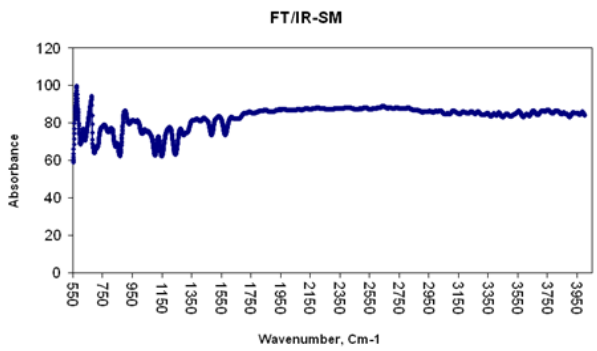

Fig. 6 FTIR-spectrum of the blank membrane before fouling

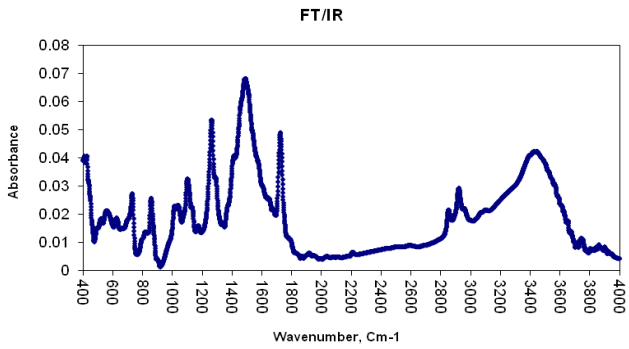

Fig. 7 FTIR-spectrum of the membrane after fouling

in Figs. 4-5. FTIR is used as a technique to obtain an infrared spectrum of absorption, emission and photo-conductivity of the fouling layer formed on the surface of the membrane before and after fouling is given in Table 2.

FTIR-spectra of both blank- and fouled membrane are given in Figs. 6-7, which confirms absorbance deficiency due to fouling.

Table 2 Elemental composition % of the membrane before and after fouling

Element	Blank membrane		Membrane after fouling	
	Weight %	Atomic %	Weight %	Atomic %
C	66.54	74.43	36.90	47.20
O	27.43	23.04	46.30	44.47
S	6.03	2.53	6.64	3.18
Na	-	-	3.60	2.40
Mg	-	-	0.51	0.32
Al	-	-	0.44	0.25
Si	-	-	0.62	0.34
P	-	-	0.14	0.07
Cl	-	-	0.35	0.15
Ca	-	-	3.68	1.41
Fe	-	-	0.11	0.03
Cu	-	-	0.39	0.09
Zn	-	-	0.33	0.08
Total	100.00	100.00	100.00	100.00

Table 3 shows the IR absorptions summary with functional groups. Imaging analysis using scanning electron microscope (SEM) coupled with Fourier transform infrared (FTIR) have shown that the composition of the fouling layer on membrane surface was dye molecules, microorganisms encased in extracellular polymers, and inorganic salts.

In addition to this examination ROIFA-4 programs (El-Manharawy and Hafez 2005) was used for the determination of inorganic fouling. The output of the program proved that the total fouling load was nearly 1.1 mM/kg in the form of 49.3% Carbonates, 10.1% Sulfates, 37.2% Silicates, 37.2% Phosphates, and 0.93% Iron oxides.

4.2 Effect of fouling on operating parameters

As shown in Fig. 8, the permeate flux (J_p) is decreased sharply to reach 40% of its initial value after 180 min. The continuous formation of bio-, inorganic-, and organic fouling layer (Cheryan 1998, Sampath *et al*. 2014) will result in a further decrease in the permeate flux (J_p) to exceed 60% after 270 min. The latter remains constant before it suffers a serious failure after 600 min.

The rejection of salts decreases with increasing fouling. It follows the same trends as the flux decline Fig. 9 and appears to be in agreement electro-kinetic potential in colloidal dispersion (zeta potential). Such layer of colloids can lead to hindered back diffusion of salts away from the membrane surface that referred to as cake-enhanced concentration polarization (Ng and Elimelech 2004, Lee *et al*. 2003, Seidel and Elimelech 2002).

Table 3 IR Absorptions Summary

Functional goup	Characteristic asorption(s) (cm^{-1})	Notes
Alkyl C-H Stretch	2950-2850 (m or s)	Alkane C-H bonds are ubiquitous and therefore usually less useful in determining the structure.
Alkenyl C-H Stretch Alkenyl C=C Stretch	3100-3010 (m) 1680-1620 (v)	Absorption peaks above 3000 cm^{-1} are frequently diagnostic of un-saturation
Alkynyl C-H Stretch Alkynyl C≡C Stretch	~3300 (s) 2260-2100 (v)	
Aromatic C-H Stretch Aromatic C-H Bending Aromatic C=C Bending	~3030 (v) 860-680 (s) 1700-1500 (m,m)	
Alcohol/Phenol O-H Stretch	3550-3200 (broad, s)	See "Free vs. Hydrogen-Bonded Hydroxyl Groups" in the Introduction to IR Spectra for more information
Carboxylic Acid O-H Stretch	3000-2500 (broad, v)	
Amine N-H Stretch	3500-3300 (m)	Primary amines produce two N-H stretch absorptions, secondary amides only one, and tertiary none.
Nitrile C≡N Stretch	2260-2220 (m)	
Aldehyde C=O Stretch Ketone C=O Stretch Ester C=O Stretch Carboxylic Acid C=O Stretch Amide C=O Stretch	1740-1690 (s) 1750-1680 (s) 1750-1735 (s) 1780-1710 (s) 1690-1630 (s)	The carbonyl stretching absorption is one of the strongest IR absorptions and is very useful in structure determination as one can determine both the number of carbonyl groups (assuming peaks do not overlap) but also an estimation of which types.
Amide N-H Stretch	3700-3500 (m)	As with amines, an amide produces zero to two N-H absorptions depending on its type.

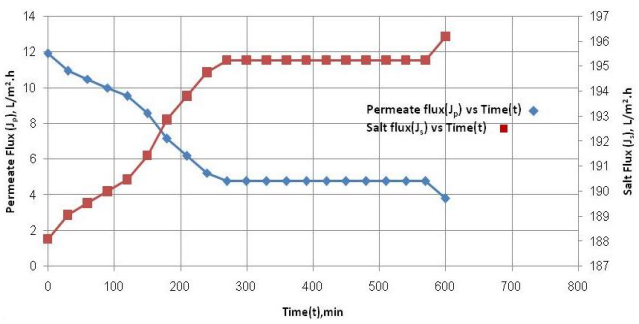

Fig. 8 Effect of fouling layer on both permeate and salt fluxes (Jp , Js)

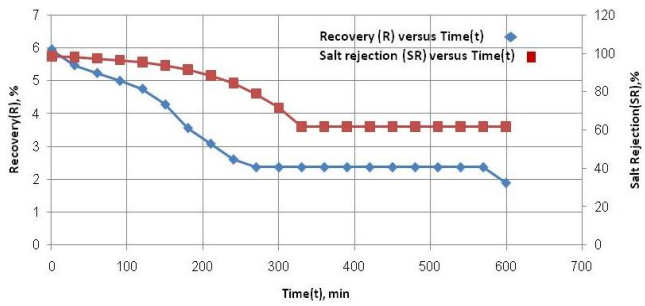

Fig. 9 Effect of fouling layer on recovery (R) and salt rejection (SR)

Solution-diffusion model predicted mass transfer parameters for experimental nanofiltration unit are illustrated in Table 4 for RB5. Proves an exponential increase and sharp decrease of the mass transfer coefficient (kp) with increasing cross flow Reynolds number and time respectively Fig. 10. It is hypothesized that for thin cake layers (compared to the film layer thickness), the cake-enhanced osmotic pressure results solely from the hindered back-diffusion of salt ions trapped within the colloid-cake layer (Hoek 1996).

The diffusion of salt ions back into the bulk is hindered due to accumulation of a thin cake layer on the membrane surface. Enhanced membrane surface salt conc. (C_m^*) is attributed to hindered back diffusion of salt ions trapped in the cake layer leading to an enhanced osmotic pressure drop across the membrane ($\Delta\pi_m^*$).

By determining the cake layer porosity (ε), the effective diffusion coefficient for salt ion strapped within the colloid deposit layer can be calculated using a simple analytical expression given by (Faibish *et al*. 1998), as shown below

$$D^* = (\varepsilon/\tau)D, \quad with \quad \tau \approx (1 - ln\varepsilon^2) \qquad (24)$$

Porosities of silica colloids cake layer formed under similar physical and chemical conditions were typically in the range of 0.3→ 0.7 (Yiantsios and Karabelas 1998, Endo and Alonso 2001, Ku *et al*. 2005). For the range of typical porosity values, the effective diffusion coefficient can be reduced to about 10 and 40% of the bulk diffusion coefficient, leading to a substantial enhanced membrane

Table 4 Solution diffusion model predicted mass transfer parameters for experimental NF unit (RB5)

Time, min	u_{eff}	Re_{eff}	k_p	K_w	K_s
0	0.411	90.401	6.1E-05	3.93E-07	4.59E08
30	0.378	83.169	5.93E05	3.61E-07	5.74E08
60	0.362	79.553	5.84E05	3.45E-07	7.47E08
90	0.345	75.937	5.75E05	3.28E-07	9.73E08
120	0.329	72.321	5.66E05	3.12E-07	1.27E07
150	0.296	65.089	5.46E05	2.8E-07	1.57E07
180	0.247	54.241	5.14E05	2.32E-07	1.82E07
210	0.214	47.009	4.9E-05	2E-07	2.2E-07
240	0.181	39.776	4.64E05	1.69E-07	2.64E07
270	0.164	36.160	4.49E05	1.52E-07	3.47E07
300	0.164	36.160	4.49E05	1.51E-07	5.16E07
330	0.164	36.160	4.49E05	1.49E-07	8.08E07
360	0.164	36.160	4.49E05	1.49E-07	8.08E07
600	0.131	28.928	4.17E05	1.19E-07	6.48E07

$$\frac{1}{k^*} = \frac{\delta_c}{D^*} + \frac{\delta_s}{D}, \quad with \quad \delta_s = \delta_f - \delta_c \tag{25}$$

Combination of Eqs. (24)-(25) proves that $(k_p/k^*) > 1$. A continuous decline of solute mass transfer coefficient with time is, therefore, expected which is proved experimentally Fig. 10.

The solution-diffusion model employs the membrane transport equations to describe the flux through the membrane (J_i) as a function of the concentration of solute in both feed and permeate and the pressure difference across the membrane (Shi *et al*. 2006)

$$J_i = D_i K_{spi} \frac{\left\{c_{if} - c_{ip} exp\left[-\frac{\vartheta_i(P_f - P_p)}{RT}\right]\right\}}{l} = D_i K_{spi} \alpha_i \tag{26}$$

$$K_{spi} = \frac{c_{sp}}{c_{dsp}} \tag{27}$$

Based on Eq. (26), the value of term $\alpha_i =$

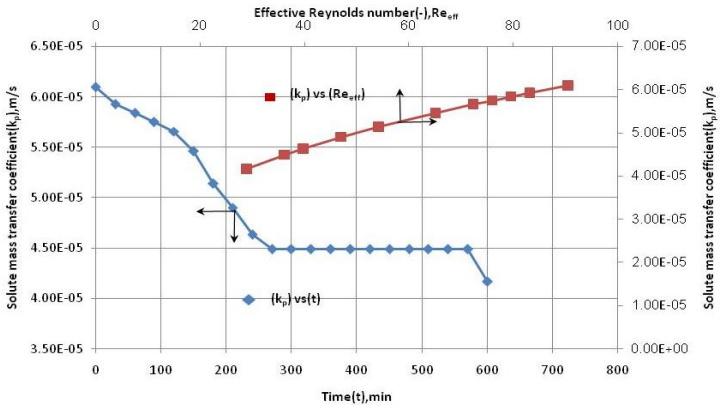

Fig. 10 Effect of fouling layer on mass transfer coefficient of dye-solute on the permeate

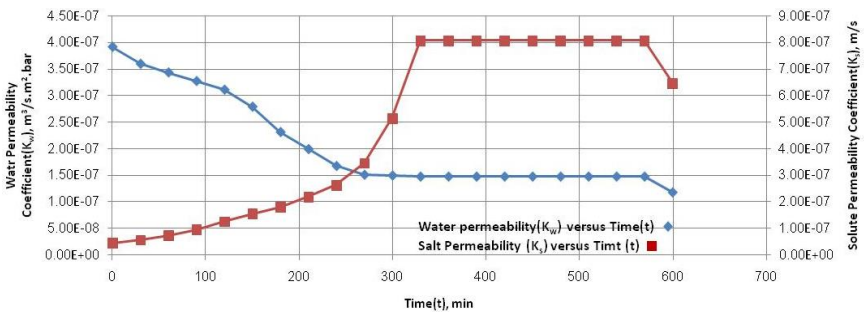

Fig. 11 Effect of fouling layer on both water and salt permeability coefficients (Kw, Ks)

surface salt concentration.

Accordingly, the effective mass transfer coefficient can be considered two separate coefficients; one coefficient describes mass transfer through the colloid deposit layer and the other coefficient accounts for mass transfer from the interface into the bulk. The resulting hindered mass transfer coefficient (k^*) is estimated from

$\frac{\left\{c_{io} - c_p exp\left[-\frac{\vartheta_i(P_f - P_p)}{RT}\right]\right\}}{l}$ is increased with decreasing permeate pressure. The membrane sorption coefficient (K_i) value and the diffusion coefficient (D_i) for each component have increased. The permeation flux change is affected by the product of (D_i) and $(K_i\alpha_i)$. This fast decrease has indicated that the value added to $(K_i\alpha_i)$ is less than the value-

subtracted from (D_i).

The direct proportionality of (D_i) with the mass transfer coefficient of the solute on the permeate side (k_p), as proved by the Sherwood number (Sh), results in a simultaneous increase of both as proved in Fig. 10.

$$Sh = \frac{k_p d_h}{D_i} \tag{28}$$

Experimental results prove the direct- and inverse-proportionality of water- and salt permeability coefficients (K_w, K_s) with permeates flux respectively (J_p). graphical presentation of the calculated K_w and K_s Eqs. (29)-(30) reveals their continuous decline and increase with time respectively Fig. 11.

5. Conclusions

The effect of membrane fouling on the performance of a Desal HL2521-TF nanofiltration unit was investigated using dye-house wastewater. Fouling is caused by the unwanted accumulation or deposition of material accompanying dye house effluent fluid on the membrane surface. Particulate fouling (caused by suspended solids), biological fouling (caused by algae, fungi and bacteria), and molecules of dyestuff material together with inorganic salts are the main reasons of membrane fouling.

At stable operating conditions, a sharp decline of permeate flux and dye-rejection was observed experimentally which is attributed to the continuous irreversible growth of foulant layer. Full characterization of the fouled membrane is accomplished by practicing a variety of instrumental EDX, FTIR, and SEM analyses. The diffusion coefficient of the dye molecules is seriously hindered by the formed colloid layer. The dye- mass transfer coefficient proves dramatic decline and increases with time and cross flow Reynolds number respectively. The total membrane lifespan over the last effective filtration period was 9.5 h.

References

Abbas, A. (2007), "On the performance limitation of reverse osmosis water desalination systems", *Int. J. Nuclear Desalination*, **2**(3), 205-218.

Abdel-Fatah, M.M.A. (2012), "Study of dye-house wastewater treatment using Nanofiltration membrane", Ph.D. Thesis; Faculty of Engineering, Cairo University, Egypt.

Abdel-Fatah, M.A., Abdel-Salam, O.E. and Abdel-Maoty, R.Z. (2017), "Regeneration of fouled nanofiltration membrane used in dye-house wastewater treatment", *J. Desalin. Water Purif.*, **7**, 14-22. http://ababilpub.com/download/jdwp7-3

Abid, M.F., Zablouk, M.A. and Abid-Alameer, A.M. (2012), "Experimental study of dye removal from industrial wastewater by membrane technologies of reverse osmosis and nanofiltration", ~~*Iranian*~~ *J. Environ. Health Sci. Eng.*, **9**, 17.

Amokrane, M., Sadaoui, D. and Dudeck, M. (2015), Effect of inter-filament distance on the improvement of Reverse Osmosis desalination process", *Proceedings of the 22th Congrès Français de Mécanique*, Lyon, France, August.

Al-Aseeri, M., Bu-Ali, Q., Haji, S. and Al-Bastaki, N. (2007), "*Removal of Acid Red and sodium chloride mixtures from aqueous solutions using nanofiltration*", *Desalination*, **206**, 407-413. https://doi.org/10.1016/j.desal.2006.03.575

Chalor, J., Supatpong M. and Ratana, J. (2007), "Influence of inorganic sealants and natural organic matter on nanofiltration membrane fouling", *J. Membrane Sci.*, **267**(1), 138-145. https://doi.org/10.1016/j.memsci.2006.10.034

Cheryan, M, (1998), *Ultrafiltration and Microfiltration Handbook*, Techno Press, Lancaster.

Chollom, M.N., Rathilal, S., Pillay, V.L. and Alfa, D. (2015), "The applicability of nanofiltration for the treatment and reuse of textile reactive dye effluent", *Water SA*, **41**(3), 398-405. http://dx.doi.org/10.4314/wsa.v41i3.12

El-Manharawy, M.S. and Hafez, A.I. (2005), "How to estimate inorganic fouling flux on RO membrane by using ROIFA-4?", *Desalination*, **277**(1-3), 407-413.

Endo, Y. and Alonso, M. (2001), "The Physical meaning of specific cake resistance and effects of cake properties in compressible cake filtration", *Filtration Sep.*, **24**(2), 283-293. https://doi.org/10.1016/S0301-9322(97)00062-1

Faibish, R.S., Elimelech, M. and Cohen, Y. (1998), "Effect of interparticle electrostatic double layer interactions on permeate flux decline in crossflow membrane filtration of colloidal suspensions: An experimental investigation", *J. Colloid Interf. Sci.*, **204**(1), 77-86.

Hoek, E.M.V. (1996), "The diffusive tortuosity of fine-grained unlithified sediments", *Geochim. Cosmochim. Acta*, **60**(16), 3139-3142. https://doi.org/10.1016/0016-7037(96)00158-5

Jain, S.K., Purkait, M.K., De, S. and Bhattacharya, P.K. (2006), "Treatment of leather plant effluent by membrane separation processes", *Separat. Sci. Technol.*, **41**(15), 3329-3348. https://doi.org/10.1080/01496390600915080

Jiang, A., Ding, Q., Wang, J., Jiangzhou, S., Cheng, W. and Xing, C. (2014), "Mathematical modeling and simulation of SWRO process based on simultaneous method", *J. Appli. Mathe.* http://dx.doi.org/10.1155/2014/908569

Jyoti, G., Keshav, A. and Anandkumar, J. (2015), "Review on pervaporation: theory, membrane performance, and application to intensification of esterification reaction", *J. Eng.* http://dx.doi.org/10.1155/2015r/927068

Karisma, D., Febrianto, G. and Mangindaan, D. (2017), "Removal of dyes from textile wastewater by using nanofiltration polyetherimide membrane", *The International Conference on Eco Engineering Development* (*ICEED 2017*), *IOP Conference Series*: *Earth and Environmental Science*, **109**(1), 012012. https://doi.org/10.1088/1755-1315/109/1/012012

Ku, Y., Lee, P.L. and Wang, W.Y. (2005), "Removal of acidic dyestuffs in aqueous solution by nanofiltration", *J. Membr. Sci.*, **250**(1-2), 159-165.

Lee, S., Cho, J. and Elimelech, M. (2003), "Influence of colloidal fouling and feed water recovery on a salt rejection of RO and NF membranes", *Desalination*, **160**(1), 1-12. https://doi.org/10.1016/S0011-9164(04)90013-6

Lee, S., Boo, C., Elimelech, M. and Hong, S. (2010), "Comparison of fouling behavior in forwarding osmosis (FO) and reverse osmosis (RO)", *J. Membr. Sci.*, **365**, 34-39. https://doi.org/10.1016/j.memsci.2010.08.036

Leo, C.P., Yeo, K.L., Lease, Y. and Derek, C.J.C. (2016), "Fouling evaluation on nanofiltration for concentrating phenolic and flavonoid compounds in propolis extract", *Membr. Water Treat., Int. J.*, **7**(4), 327-339. https://doi.org/10.12989/mwt.2016.7.4.327

Masmoudi, G., Trabelsi, R., Ellouze, E. and Amar, R.B. (2014), "New treatment at source approach using combination of microfiltration and nanofiltration for dyeing effluents reuse", *Int. J. Environ. Sci. Technol.*, **11**, 1007-1016. https://doi.org/10.1007/s13762-013-0303-3

Mohammad, A.W., Teow, Y.H., Ang, W.L., Chung, Y.T., Oatley-Radcliffe, D.L. and Hilal, N. (2015), "Nanofiltration membranes

review: Recent advances and future prospects", *Desalination*, **356**, 226-254. https://doi.org/10.1016/j.desal.2014.10.043

Murthy, Z.V.P. and Chaudhari, L.B. (2009), "Treatment of distillery spent wash by combined UF and RO processes", *Global NEST J*., **11**(2), 235-240.

Ng, H.Y. and Elimelech, M. (2004), "Influence of colloidal fouling on a rejection of trace organic contaminants by reverse osmosis", *J. Membr. Sci*., **244**(1-2), 215-226. https://doi.org/10.1016/j.memsci.2004.06.054

Rabiller-Baudry, M., Le Maux, M., Chaufer, B. and Begoin, L. (2002), "Characterization of cleaned and fouled membrane by ATR-FTIR and EDX analysis coupled with SEM", *Desalination*, **146**, 123-128. https://doi.org/10.1016/S0011-9164(02)00503-9

Rashidi, H.R., Sulaiman, N.M.N., Hashim, N.A., Hassan, C.R.C. and Ramli, M.R. (2015), "Synthetic reactive dye wastewater treatment by using nano-membrane filtration", *Desalinat. Water Treat*., **55**(1), 86-95. https://doi.org/10.1080/19443994.2014.912964

Rowe, B.W., Robeson, L.M., Freeman, B.D. and Paul, D.R. (2010), "Influence of temperature on the upper bound: Theoretical considerations and comparison with experimental results", *J. Membr. Sci*., **360**, 58-69. https://doi.org/10.1016/j.memsci.2010.04.047

Sampath, M., Shukla, A. and Rathore, A.S. (2014), "Modeling of filtration processes—microfiltration and depth filtration for harvest of a therapeutic protein expressed in Pichia pastoris at constant pressure", *Bioengineering*, **1**, 260-277. http://dx.doi:10.3390/bioengineering1040260

Schaefer, A., Fane, A.G. and Waite, T.D. Eds. (2005), *Nanofiltration Principles and Applications*, Elsevier, Oxford, UK; New York, USA.

Schneider, R.P., Ferreira, L.M., Binder, P. and Ramos, J.R. (2005), "Analysis of foulant layer in all elements of an RO train", *J. Membr. Sci*., **261**, 152-162. https://doi.org/10.1016/j.memsci.2005.03.044

Seidel, A. and Elimelech, M. (2002), "Coupling between chemical and physical interactions in natural organic matter fouling of nanofiltration membranes; implications for fouling control", *J. Membr. Sci*., **203**(1-2), 245-255. https://doi.org/10.1016/S0376-7388(02)00013-3

Shi, D., Kong, Y., Yu, J., Wang, Y. and Yang, J. (2006), "Separation performance of polyimide nanofiltration membranes for concentrating spiramycin extract", *Desalination*, **191**(1-3), 309-317.

Standard Methods (1992), Examination of Water and Wastewater, (18th Edition), American Public Health Association.

Thamaraiselvan, C. and Noel, M. (2015), "Membrane processes for dye wastewater treatment: recent progress in fouling control", *Critical Rev. Environ. Sci. Technol*., **45**(10), 1007-1040. https://doi.org/10.1080/10643389.2014.900242

Xu, P., Drewes, J.E., Kim, T.U., Bellona, C. and Amy, G. (2006), "Effect of membrane fouling on a transport of organic contaminants in NF/RO membrane applications", *J. Membr. Sci*., **279**, 165-175. https://doi.org/10.1016/j.memsci.2005.12.001

Xuan Nguyen, H. and Van der Bruggen, B. (2015), "Nanofiltration of synthetic and industrial dye baths: Influence of temperature on rejection and membrane fouling", *J. Membr. Sci. Res*., **1**, 34-40. https://doi.org/10.22079/JMSR.2015.12304

Yiantsios, S.G. and Karabelas, A.J. (1998), "The effect of gravity on the deposition of micron-sized particles on smooth surfaces", *Int. J. Multiphase Flow*, **24**, 283-293.

Zhao, Y., Taylor, J.S. and Chellam, S. (2005), "Predicting RO/NF water quality by modified solution diffusion model and artificial neural networks", *J. Membr. Sci*., **263**, 38-46. https://doi.org/10.1016/j.memsci.2005.04.004

CC

Nomenclature

- A = Membrane area (m^2)
- A_{eff} = Effective area (m^2)
- b = Leafwidth (m)
- c_{if} = Concentration of component in the feedstock (mg/l)
- c_{ip} = Concentration of component in the permeate (mg/l)
- c_{sp} = Concentration of adsorbateon the membrane at equilibrium
- $(mol/kg)c_{dsp}$ = Total dissolved adsorbate concentration remaining in the solution
- at equilibrium ($^{mol}/_{m^3}$)
- $\bar{C}$ = Average salinity on the feedside (mg/l)
- C_f = Dye/salt feed concentration (mg/l)
- C_c = Concentrate concentration (mg/l)
- C_p = Permeate concentration (mg/l)
- d_h = Hydraulic diameter (m^2)
- D = Soluted diffusion coefficient in water (m^2/s)
- DR = Dye rejection (%)
- h = Channel height (m^2)
- h_{sp} = Spacer thickness (m^2)
- J_p = Permeate flux ($l/m^2.h$)
- J_s = salt flux ($kg/m^2.h$)
- k = Mass transfer coefficient (m/s)
- k_p = Permeate − side mass transfer coefficient (m/s)
- K_{sp} = Membrane sorption coefficient (m^3/kg)
- K_s = Salt permeability coefficient (m/s)
- K_w = Water permeability coefficient ($m^3/m^2.s.bar$)
- l = Membrane thickness (m)
- L = Channel length (m)
- M_s = Rateof solid flow through the membrane (kg/s)
- NDP = Net driving pressure (bar)
- P = Operating pressure (bar)
- ΔP = Net hydraulic pressure differential across the membrane(bar)
- $\bar{P}$ = Average hydraulic pressure on the feed side (bar)
- P_f = Hydraulic pressure on the feed side (bar)
- P_p = Hydraulic pressure on the permeate side (bar)
- P_c = Hydraulic pressure on the concentrate side (bar)
- $(P_f - P_p)$ = Pressure difference across the membrane (bar)
- Q_f = Feed flowrate (l/h)
- Q_c = Concentrate flowrate (l/h)
- Q_p = Peremeate flowrate (l/h)
- R = Universal gas constant ($bar.m^3/mol.$°C)
- Re_{eff} = Effective cross flow Reynolds number on permeate side(−)
- Re_c = Effective cross flow Reynolds numberon concentrate side(−)
- R_m = Membrane hydraulic resistance (m^{-1})
- $R_{non-rec}$ = Anynon − recoverable resistance developed during filtration (m^{-1})
- S_{fc} = Wettedsur face of the flat channel (m^2)
- S_{sp} = Wetted surface of the spacer (m^2)
- Sc = Schmidt number (−)
- Sh = Sherwood number (−)
- SR = Salt rejection (%)
- T = Operating temperature (°C)
- U = Fluid linear velocity ($^m/_s$)
- u_{eff} = Effective cross flow fluid velocity ($^m/_s$)
- V_{fc} = Volume of the flat channel (m^3)
- V_{Tot} = Total volume (m^3)
- V_{sp} = Volume of the spacer (m^3)

Greek symbols

- ρ = Fluid density ($^{kg}/_{m^3}$)
- μ = Dynamic viscosity of the solution ($kg.m^{-1}.s^{-1}$)
- σ = Osmotic reflection coefficient (−)
- ϑ_i = Molar volume of component (m^3/mol)
- $\Delta\pi$ = Net osmotic pressure differential across the membrane (bar)
- $\bar{\pi}$ = Average osmotic pressure on the feed side (bar)
- π_f = Osmotic pressure on the feed side (bar)
- π_p = Osmotic pressure on the permeate side (bar)
- π_c = Osmotic pressure on the concentrate side (bar)
- ε = Porosity (−)
- δ_c = colloid deposit layer thickness( )
- δ_f = film layer thickness (m)